Journal of Sol-Gel Science and Technology (2019) 89:785–795
https://doi.org/10.1007/s10971-018-4897-2

ORIGINAL PAPER: SOL-GEL AND HYBRID MATERIALS FOR OPTICAL, PHOTONIC AND OPTOELECTRONIC APPLICATIONS

Mesoporous silica modified luminescent Gd_2O_3:Eu nanoparticles: physicochemical and luminescence properties

Ali Aldalbahi[1,2] · Mostafizur Rahaman[2] · Anees A. Ansari[1]

Received: 21 September 2018 / Accepted: 26 November 2018 / Published online: 7 December 2018

Abstract

Highly colloidal Gd_2O_3:Eu nanoparticles (core-NPs) were synthesized by thermal decomposition via weak base at low temperature. The sol–gel chemical process was employed for silica layer surface coating to increase solubility, colloidal stability, biocompatibility, and non-toxicity at the ambient conditions. XRD results indicate the highly purified, crystalline, single phase, and cubic phase Gd_2O_3 nanocrystals. TEM image shows that the mesoporous thick silica layer was effectively coated on the core nanocrystals, which have irregular size with nearly spherical shape and grain size about 10–30 nm. An absorption spectra and zeta potential results in aqueous media revealed that solubility, colloidal stability, and biocompatibility character were enhanced from core to core–shell structure because of silica layer surface encapsulation. The samples, demonstrated excellent photoluminescence properties (dominant emission $^5D_0 \rightarrow {}^7F_2$ transition in the red region at 610 nm), indicated to be used in optical bio-detection, bio-labeling, etc. The photoluminescence intensity of the silica shell modified core/shell NPs was suppressed relatively core-NPs; it indicates the multi-photon relaxation pathways arising from the surface coated high vibrational energy molecules of the silanol groups. The core/$nSiO_2$/$mSiO_2$ nanocrystals display strong emission ($^5D_0 \rightarrow {}^7F_2$) transition along with excellent solubility and biocompatibility, which may find promising applications in the photonic based biomedical field.

Graphical Abstract

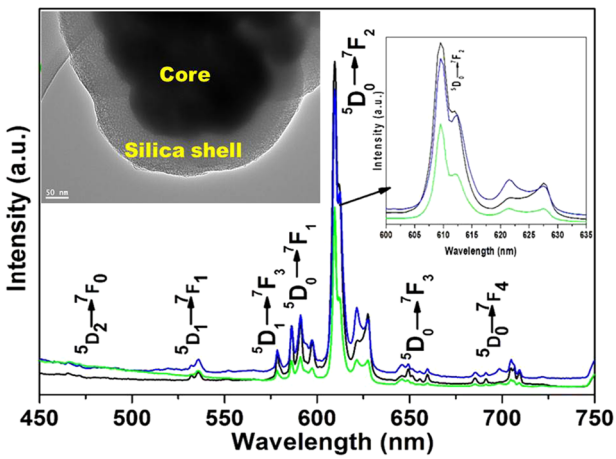

✉ Ali Aldalbahi
aaldalbahi@ksu.edu.sa

✉ Anees A. Ansari
aneesaansari@gmail.com

[1] King Abdullah Institute for Nanotechnology, King Saud University, Riyadh 11451, Saudi Arabia

[2] Department of Chemistry, College of Science, King Saud University, Riyadh 11451, Saudi Arabia

Highlights

- Multi-silica layers coated luminescent Gd_2O_3:Eu@nSiO_2@mSiO_2 core–shell nanoparticles.
- Mesoporous, highly aqueous dispersible core-shell nanoparticles.
- Impact of silica shell on physiochemical properties.
- Excellent absorbance and photoluminescence properties.

Keywords Gadolinium oxide · Mesoporous · silica · Biocompatible · Zeta potential · Luminescence properties

1 Introduction

In recent years, luminescent rare-earth inorganic materials have aroused rapidly growing interest for fluorescent-based biomedical applications because of their unique optical properties such as sharp absorption and emission lines invisible region, low phonon energy, good quantum yield, narrow bandwidth, large stocks shift, high photochemical and thermal stability, excellent biocompatibility, and non-toxicity [1–5]. These outstanding optical and photochemical properties make them promising candidates for their future applications in widespread biomedical sciences. Amongst lanthanide nanomaterials, gadolinium oxide (Gd_2O_3) is an ideal host matrix for doping of luminescent ion due to their excellent photochemical and thermal stability and low vibrational energy [1–3, 5–7]. Additionally, Gd_2O_3 is magnetically active and used as magnetic resonance imaging contrast agent [2–4, 8]. Therefore, trivalent Eu substituted Gd_2O_3 is one of the most important red-emitting inorganic material because of its significant emission and exciton in UV/Visible regions [3, 4, 7]. Many efforts were made for the synthesis of Gd_2O_3 materials through various chemical routes such as polyol [9, 10], sono-chemical [11], microemulsion [12], sol-gel chemical [13], microwave decomposition [14, 15], thermal decomposition [16, 17], hydrothermal/solvothermal [18–20], co-precipitation [21–23], and aqueous self-combustion process. Among them, low-temperature thermal decomposition process can be the most efficient and appropriate synthesis route as it can yield high phase purity powder with excellent chemical homogeneity. So that, micro to nano-scale Gd_2O_3:Ln synthesis methods with different morphologies via wet chemical process are considered better for their molecular level proper mixing. This is because molecular level homogeneous mixing offers the possibilities for controlling the chemical composition, obtaining better-quality homogeneity, single phase, and higher surface area powders. Instead of ammonia or sodium hydroxide based co-precipitation process, urea-based thermal decomposition method is also considered as a better process [24–28]. Urea-based thermal decomposition process has an additional advantage; homogeneous precipitation generates fine small particles, which have a relatively narrow size distribution with the large surface area and high porosity compared to others. Additionally, it takes advantage of the exothermic, fast, and self-sustaining chemical reactions between lanthanide nitrates/chlorides and the weak base (Urea) reducing agent. As a consequence, it is particularly highly suitable for the elaboration of uniform nanocrystalline particles of lanthanides with the high specific surface area and superfine dimensions.

In the present study, we illustrated the single step procedure for the synthesis of europium-doped gadolinium oxide nanoparticles (Core-NPs) via thermal decomposition process at low temperature with grain size about 10–30 nm, which were well monodispersed and showed high dispersibility in aqueous media. Consequently, the prepared core-NPs were covered through amorphous silica layer to improve their solubility, biocompatibility, and toxicity character at ambient conditions. These core and silica surface modified core–shell NPs were fully characterized systematically via different physio-chemical techniques such as X-ray diffraction pattern (XRD), transmission electron microscopy (TEM), energy dispersive x-ray analysis (EDX), thermogravimetric analysis (TGA), and zeta potential, Fourier transform infrared (FTIR), UV/Visible, excitation and emission spectroscopy to examine their crystallinity, phase purity, crystal structure, surface morphology, thermal durability, surface chemistry, solubility, biocompatibility optical absorption, and photoluminescence properties. For their use in biomedical sciences, it is necessary to functionalized or cover the surface with active functional groups to enhance their aqueous solubility character, which can be easily available for binding with bio-macromolecules as per requirement. For surface coating or functionalization, silica shell coating process is well accepted to grow on the surface of the luminescent core-NPs by co-hydrolysis and poly-condensation with tetraethyl-orthosilicate (TEOS) [10, 29, 30]. The surface grew SiO_2 layer is easily available for binding with other –OH groups of bio-macromolecules by condensation to form a Si–O–Si network; it would be applicable for highly fluorescent, sensitive, and reproducible biomedical applications. Additionally, the surface functionalized NPs with the high surface area and mesoporosity allow for designing multifunctional systems for simultaneous drug delivery and cell imaging.

2 Experimental

2.1 Materials

Gd_2O_3 (99.99%, BDH Chemicals, UK), Eu_2O_3 (99.99%, AlfaAesar, Germany), NH_4OH, NaOH, ethyl alcohol, urea, tetraethyl-orthosilicate (TEOS), and N-cetyltrime thylammonium bromide (CTAB) were used directly as-received without further purification. Gadolinium nitrate and europium nitrate were prepared by dissolving the corresponding metal oxides in the diluted nitric acid. Milli-Q (Millipore, Bradford, USA) water was used for the synthesis and characterization of the samples.

2.2 Synthesis of Gd_2O_3:Eu (Core), Gd_2O_3:Eu@$nSiO_2$ (Core/$nSiO_2$) and Gd_2O_3:Eu@ $nSiO_2$@$mSiO_2$ (core/$nSiO_2$/$mSiO_2$)NPs

In a typical procedure for the synthesis of Gd_2O_3:Eu NPs (core), 4.5 g gadolinium nitrate hexahydrate (9.5 ml, 2 M) and 0.223 g europium nitrate hexahydrate (0.05 ml, 2 M) were mixed together in 100 ml dist. water and kept on a hot plate at 80 °C under constant mechanical stirring. Then an appropriate amount of urea, dissolved in aqueous medium was introduced into the vigorously stirred solution mixture. After that, the transparent solution mixture was transferred into round bottle flask and refluxed at 150 °C for 3–4 h. The obtained white precipitate was separated by centrifugation, washed several times with distilled water, and dried in an oven overnight. This dried sample was further calcined at 750 °C under air condition. Stober sol-gel chemical method was followed for nanoporous silica ($nSiO_2$) surface coating as discussed in the previously published literature [10, 29, 30]. In this method, 100 mg luminescent nanoparticles were treated with C_2H_5OH by ultra-sonication for half-an-hour and separated by centrifugation. The mixture was again re-dispersed in a mechanically stirred aqueous solution containing ethanol (80 ml), H_2O (25 ml), and NH_4OH (1.0 ml). Later TEOS (1.0 ml) solution was slowly introduced into the vigorously magnetically stirred solution. The reaction was proceeding for 5–6 h at environmental conditions. For mesoporous silica ($mSiO_2$) surface coating, the modified sol–gel method was applied. A solution of 100 mg Gd_2O_3:Eu@$nSiO_2$, 100 mg CTAB and 50 mg NaOH was made by dissolving in 250 ml distilled water on a hot plate at 80 °C with constant mechanical stirring [31–35]. Afterward 1.0 ml TEOS was introduced slowly into the vigorously mechanically stirred solution. The mixed solution was allowed to co-hydrolyze and condensate for 2 h to give a white precipitate, which was separated by centrifugation, washed several times with water, and dried in an oven to yield the mesoporous core–shell/SiO_2 NPs.

2.3 Characterization

Powder X-ray diffraction pattern (PANalytical X'Pert, X-ray diffractometer) equipped with Ni filter Cu$K\alpha$ ($\lambda = 1.5404$ Å) radiation was used for examining the phase purity and crystal structure of the samples. Field emission-transmission electron microscope (FE-TEM, JEM-2100F, JEOL, Japan), equipped with EDX analysis, operating at an accelerating voltage 200 kV, was applied for morphology inspection. Zeta potential was measured from zeta sizer (Brookhaven Instruments Corporation Holtsville, NY, USA). Thermal analysis was carried out by a thermo-gravimetric analyzer (Mettler Toledo, Analytical CH-8603 Schwarzenbach, Switzerland). FTIR spectra were measured from Vertex 80 (Bruker, USA) infrared spectrometer with KBr pellet technique. Absorption spectra were recorded by Cary 60 (Agilent Technologies, USA) UV–Vis spectrophotometer within the wavelength range 200–600 nm. Photoluminescence spectra were obtained from Fluorolog 3 (Model: FL3-11, Horiba Jobin Yvon, USA) photoluminescence spectrophotometer.

3 Results and discussion

X-ray diffraction pattern was reported to determine the phase purity, crystal structure, and crystallinity of the as-prepared samples. Figure 1 illustrates the XRD pattern of Gd_2O_3:Eu core, core/$nSiO_2$ and core/$nSiO_2$/$mSiO_2$ samples. All reflection peaks in all three diffractograms are well

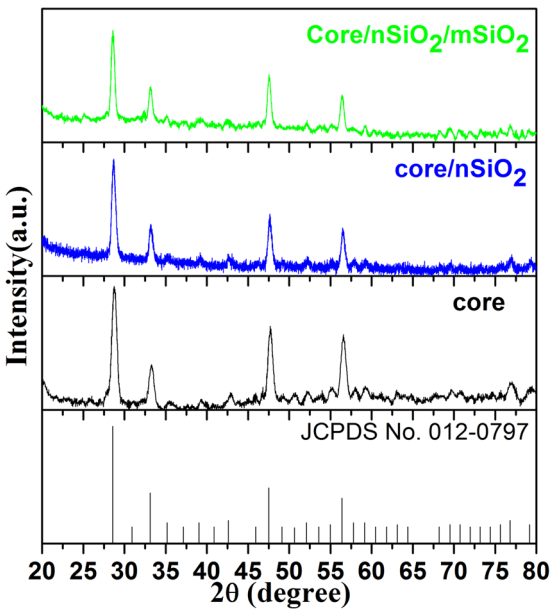

Fig. 1 X-ray diffraction pattern of Core, Core/$nSiO_2$ and Core/$nSiO_2$/$mSiO_2$ NPs

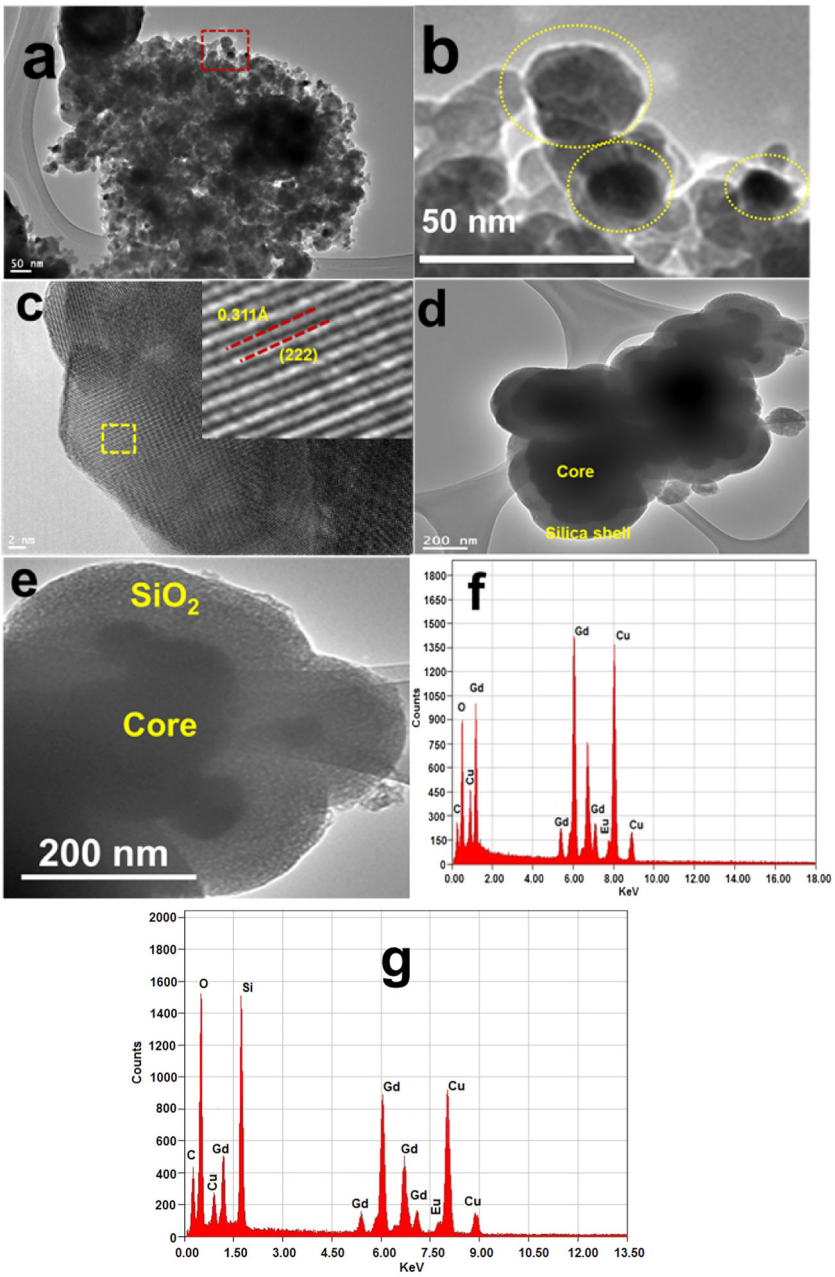

Fig. 2 TEM images of **a** low magnification core **b** high magnification core **c** lattice fringes in core image **d** low resolution core/$nSiO_2$/$mSiO_2$ image **e** high magnification core/$nSiO_2$/$mSiO_2$ image **f** EDX spectrum of core and **g** EDX spectrum of core/$nSiO_2$/$mSiO_2$ NPs

indexed to the JCPDS card No. 012-0797 that resulted cubic Gd_2O_3 phase [3, 4, 6, 36, 37]. No impurity is detected over the entire XRD range. This indicated that the Eu^{3+} ion is homogeneously distributed inside the crystal lattice and there is the formation of single phase pure cubic Gd_2O_3 NPs. The observed broadening of reflection peak width is related to the nanocrystalline size of the as-synthesized samples. An observed reduction in reflection peak intensity is implying the influence of amorphous silica surface coating on the luminescent core-NPs [38]. The most prominent diffraction peak, observed at $2\theta = 28.79^{o}$ is used for calculating the average grain size of the NPs. The experimentally estimated the crystalline size of the core, core/$nSiO_2$, and core/$nSiO_2$/$mSiO_2$ NPs are to be 10, 19, and 35 nm, respectively.

Morphology of the as-synthesized core, core/$nSiO_2$ and core/$nSiO_2$/$mSiO_2$ NPs was determined from TEM micrographs. TEM image in Fig. 2a illustrates the highly aggregated, quasi-spherical shaped, well distributed, porous, crystalline NPs with grain size about 10–30 nm. As seen in typical high-resolution TEM micrographs, spherical-shaped NPs have a large number of pores, which are randomly arranged and distributed homogeneously throughout the entire particle. This high porosity of the luminescent NPs is facilitating insolubility and high colloidal stability in an aqueous environment. We expected that the existence of the

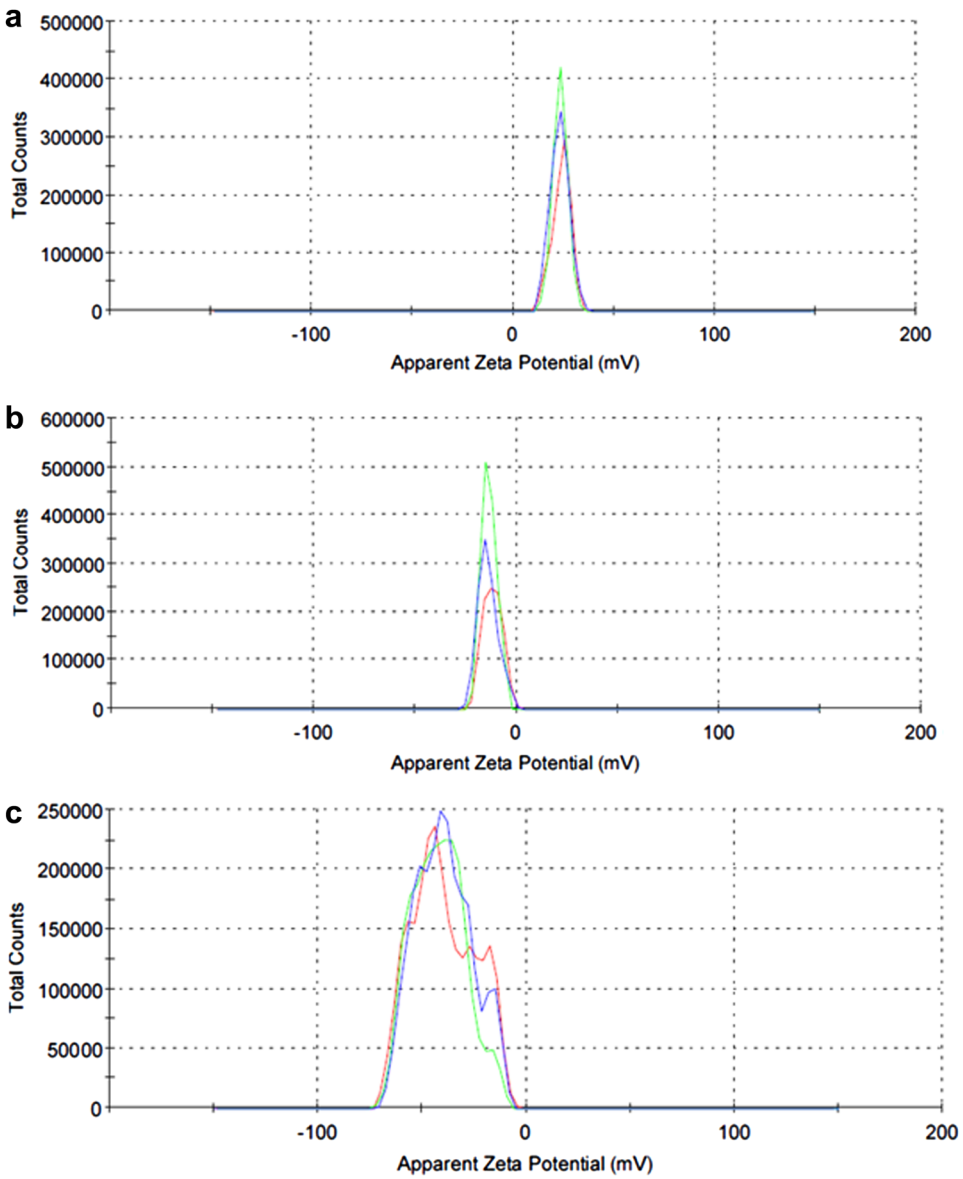

Fig. 3 Zeta-potential graphs of **a** core **b** core/nSiO_2, and **c** core/nSiO_2/mSiO_2 NPs

little amount of urea and surfactants enhanced the aggregation or clustering of the spherical shaped NPs. The lattice fringes in individual NPs are obvious as observed in the high-resolution TEM image (Fig. 2c), suggests the highly crystalline nature of the materials. The lattice planes are well separated and possessed a uniform lattice structure with the well-indexed lattice fringes $d_{222} = 0.311$ Å, which is well consistent with the d-spacing value of (222) lattice planes of the cubic phase Gd_2O_3 structure. This value is corroborated with the reported value for Gd_2O_3 NPs (Fig. 2c) [39–41]. As observed in Fig. 2d, e, a uniform and thick mesoporous silica layer possess a wormhole-channel like structure with a thickness of 55 nm that has been effectively grown over the surface of luminescent core-NPs. As seen in Fig. 2d, after encapsulation of silica layer around the core NPs, the morphology of the core NPs is still maintained; this indicates that mesoporous silica layer has no side effect on the uniformity of the core NPs. The mesoporous silica shell is a contrast in color due to different electron penetrability between the core and an amorphous silica layer. The silica shell is light gray and the core is dark black in color (Fig. 2e). EDX analysis was performed to verify the doping constituents and silica surface coating surrounding the luminescent core-NPs. The EDX profile confirmed the existence of gadolinium (Gd), oxygen (O), and europium (Eu) in the core NPs, suggesting the Eu^{3+} ion is homogeneously distributed inside the Gd_2O_3 crystal lattice (Fig. 2f, g). An additional peak of silica is observed in core/nSiO_2/mSiO_2 NPs at around 1.8 keV, indicate the successful silica coating around the core-NPs. The appearance of strong C and Cu peak in the spectra is belonging to the carbon coated copper grid. No other assigned peaks are

detected in both EDX spectrums; it suggests the phase purity of the NPs.

The solubility character, colloidal stability, and surface charge of the as-synthesized luminescent NPs were further verified from zeta potential. As illustrate in Fig. 3, the zeta potential values of core and core/$nSiO_2$ NPs at physiological pH (pH = 7.0) are 22.8 and −14.2 mV, respectively (Fig. 3a, b). Additionally, on increasing the pH values from 8 to 10 in aqueous solution, the zeta potential values gradually decrease to −13.9 and −19.9 mV, respectively (data not shown); whereas, the zeta potential values for silica modified core/$nSiO_2$/$mSiO_2$ NPs at 8 and 10 pH are −39.5 and −34.2 mV, respectively (Fig. 3c, d). Notably, the zeta potential value in core/$nSiO_2$/$mSiO_2$ NPs is greatly decreased with respect to the core-NPs. It suggests the successful silica surface modification on the luminescent core-NPs [42–44]. It is a fact that mesoporous silica is having abundant surface hydroxyl groups and provides powerful claw for easily binding with hydroxyl groups or bio-macromolecules [38, 42, 45, 46]. On increasing the pH value, the concentration of hydroxyl ion is increased, and these free hydroxyl (OH^-) ions bind with positively charged silica modified core/$nSiO_2$/$mSiO_2$ NPs to form neutralized complex, which resulted in the continuous decrease of zeta potential values [1, 42, 43]. These facts obviously confirm the solubility and excellent colloidal stability character across a broad range of pH values and further verified the surface charged over the core and surface functionalized core/$nSiO_2$/$mSiO_2$ NPs [38, 42, 46].

Thermal analysis was performed to analyze the surface adsorbed organic moieties and thermal stability of the as-synthesized NPs. The thermogram of core and core/$nSiO_2$ NPs demonstrate two-stage thermal decomposition. The first weight loss approximately 2% in core-NPs occurs between 50 and 287 °C, which seems to the removal of surface adsorbed residual water molecules and organic moieties (Fig. 4). In the second stage, approximately 4% weight loss is observed in between 288 and 800 °C, which corresponds to the combustion and elimination of surface capping oxygen species along with bulk oxygen species and formation of Gd_2O_3 nano-product; whereas, in the case of core/$nSiO_2$ NPs, initial weight loss (4%) is recorded below 200 °C. This implies the removal of surface adsorbed residual water molecules and organic moieties during silica shell formation. After that, a continuous weight loss is observed and the highest weight loss (9.2%) is recorded at 800 °C, which denotes the burning and elimination of surface modified silica [47]. It concluded that most of the organic and surface modified silica materials are decomposed before temperature reached 800 °C and the remaining product is an as-synthesized luminescent metal oxide.

The silica surface coating was further validated by FTIR spectra with the characteristic peaks of amorphous

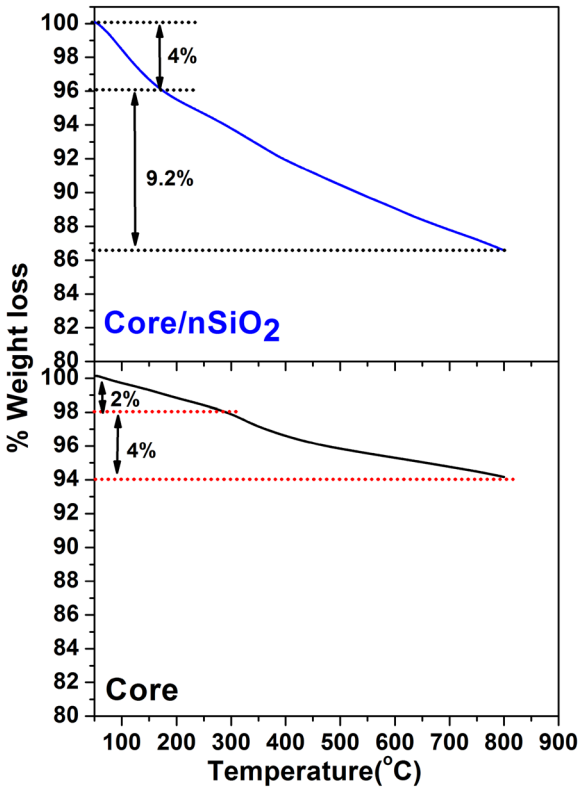

Fig. 4 Thermo-gravimetric analysis of core and core/$nSiO_2$ NPs

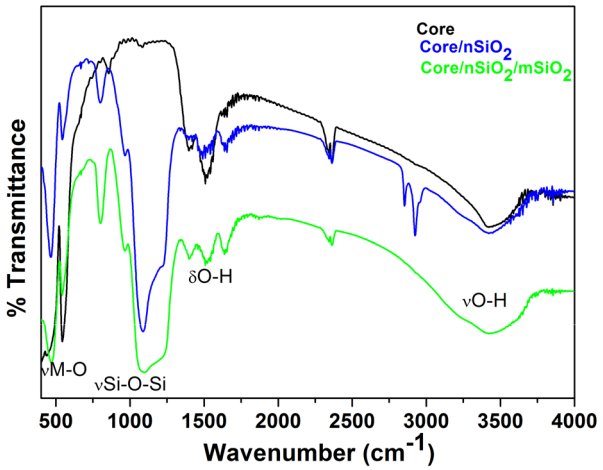

Fig. 5 UV–vis absorption spectra of Core and Core/$nSiO_2$ NPs suspended in de-ionized water

silica molecules. Compared with the infrared spectrum of Core sample, $nSiO_2$ and $mSiO_2$ coated samples have doublet high-intensity band located at 1097 cm^{-1} along with weak sharp intensity bands at 798 and 600 cm^{-1}, which are originating from stretching and bending vibrational modes of Si–O–Si, Si–O, and Si–OH surface modified amorphous silica (Fig. 5) [48–53]. A diffused broad intensity band is observed in all three spectra

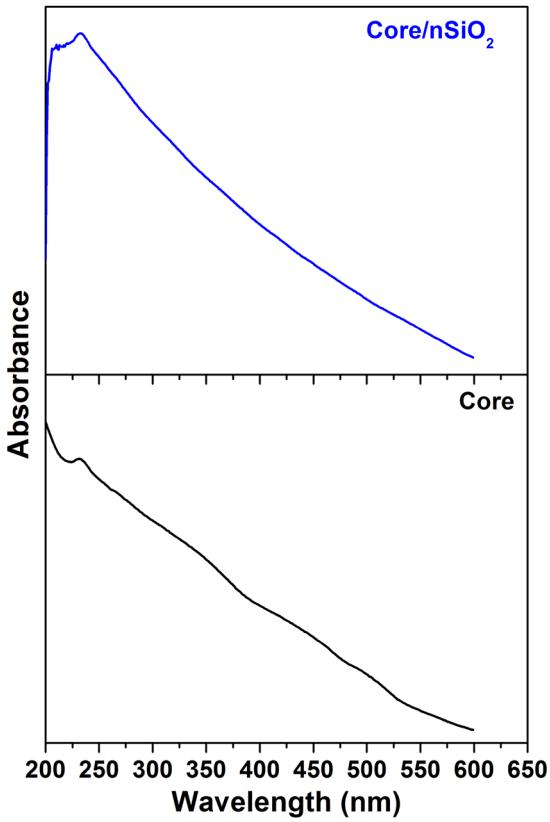

Fig. 6 FTIR spectra of the as-prepared core, core/nSiO$_2$ and core/nSiO$_2$/mSiO$_2$ NPs

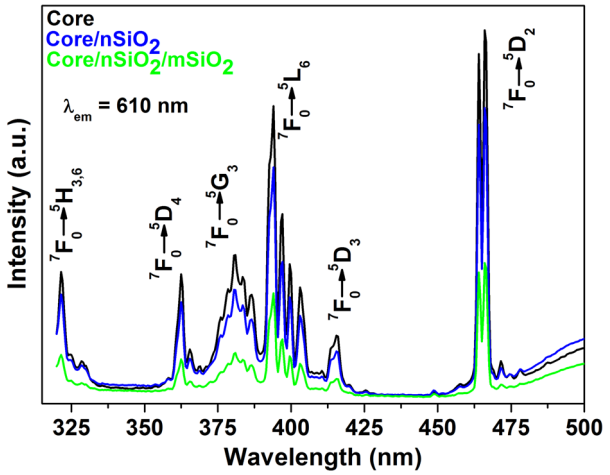

Fig. 7 Excitation spectra of the as-prepared core, core/nSiO$_2$, and core/nSiO$_2$/mSiO$_2$ NPs

located at 3425 cm^{-1} along with middle-intensity infrared band located at 1517 and 1405 cm^{-1} are ascribed to the stretching and bending vibrational modes of surface adsorbed residual water molecules [29, 33, 43, 54]. These observations are supported well with the results of XRD, TEM, EDX, and TGA analysis and previously published literature reports [9, 42, 43, 51, 52]. A sharp infrared absorption peak is observed at 549 cm^{-1} in all three spectra, which is attributed to the stretching vibration of the M-O network [55]. Optical absorption spectra were performed to investigate the optical properties, solubility, and colloidal stability character in an aqueous environment. Absorption spectra of core and core/nSiO$_2$ NPs were recorded in dist. water (Fig. 6). The core/nSiO$_2$ NPs sample exhibits strong absorbance in the visible region, which is assigned to the $^8S_{7/2} \rightarrow {}^6I_j$ transition of Gd(III) ion and existence of the amorphous silica surrounding the core-NPs [29, 32, 45, 56].

Photoluminescence measurement was performed to confirm the Eu(III) ion doping and amorphous silica surface modification around the core-NPs. Figure 7 illustrates the excitation spectra of core, core/nSiO$_2$ and core/nSiO$_2$/mSiO$_2$ NPs under monitoring 610 ($^5D_0 \rightarrow {}^7F_2$) nm emission wavelength at room temperature. The excitation spectra consist of several sharp excitation electronic transitions assigned to $^7F_0 \rightarrow {}^5H_{3,6}$(321), $^7F_0 \rightarrow {}^5D_4$(362), $^7F_0 \rightarrow {}^5G_3$(381), $^7F_0 \rightarrow {}^5L_6$(394), $^7F_0 \rightarrow {}^5D_3$ (415), and $^7F_0 \rightarrow {}^5D_2$(466), which are originating from 4*f*-4*f*-intra-configurationally transitions of Eu^{3+} ions [30, 37, 47, 54, 57–59]. Figure 8 demonstrates the emission spectra of core, core/nSiO$_2$ and core/nSiO$_2$/ mSiO$_2$ NPs upon excitation at 395 nm at room temperature. The obtained spectra display characteristic emission transitions of Eu^{3+}ions at 464-474 ($^5D_2 \rightarrow {}^7F_0$), 531-538 ($^5D_1 \rightarrow {}^7F_1$), 578($^5D_1 \rightarrow {}^7F_3$), 585-599 ($^5D_0 \rightarrow {}^7F_1$), 605-631 ($^5D_0 \rightarrow {}^7F_2$), 644-662 ($^5D_0 \rightarrow {}^7F_3$), and 684-712 ($^5D_0 \rightarrow {}^7F_4$) transitions, respectively [6, 29, 30, 47, 59, 60]. Some weak intensity emission transitions located at 470 and 535 nm assigned to $^5D_2 \rightarrow {}^7F_0$ and $^5D_1 \rightarrow {}^7F_1$ transition of the Eu^{3+} ion. This indicates low vibrational energy of the Gd–O band [6, 58]. Consequently, the multiphonon relaxation by gadolinium-oxygen vibration is not able to bridge the gaps between the higher energy levels of $^5D_2 \rightarrow {}^7F_0$ and $^5D_1 \rightarrow {}^7F_1$ transition and the $^5D_0 \rightarrow {}^7F_J$ level of Eu(III) ion completely, resulting in the emission from these levels [59]. A prominent emission transition is observed between 605 and 630 nm because of $^5D_0 \rightarrow {}^7F_2$ forced electric dipole transition and is hypersensitive to the environment [30, 47, 60]. The emission band observed around 585-598 nm is assigned to magnetic dipole transition, which is weak with respect to forced electric dipole transition [30, 60]. It is a fact that forced electric dipole transition ($^5D_0 \rightarrow {}^7F_2$) is sensitive to the surrounding chemical environment; whereas, magnetic dipole transition ($^5D_0 \rightarrow {}^7F_1$) is independent of the surrounding environment [30, 47, 60, 61]. It is obvious from the emission spectra of all three samples that the emission efficiency of hypersensitive transition or electric

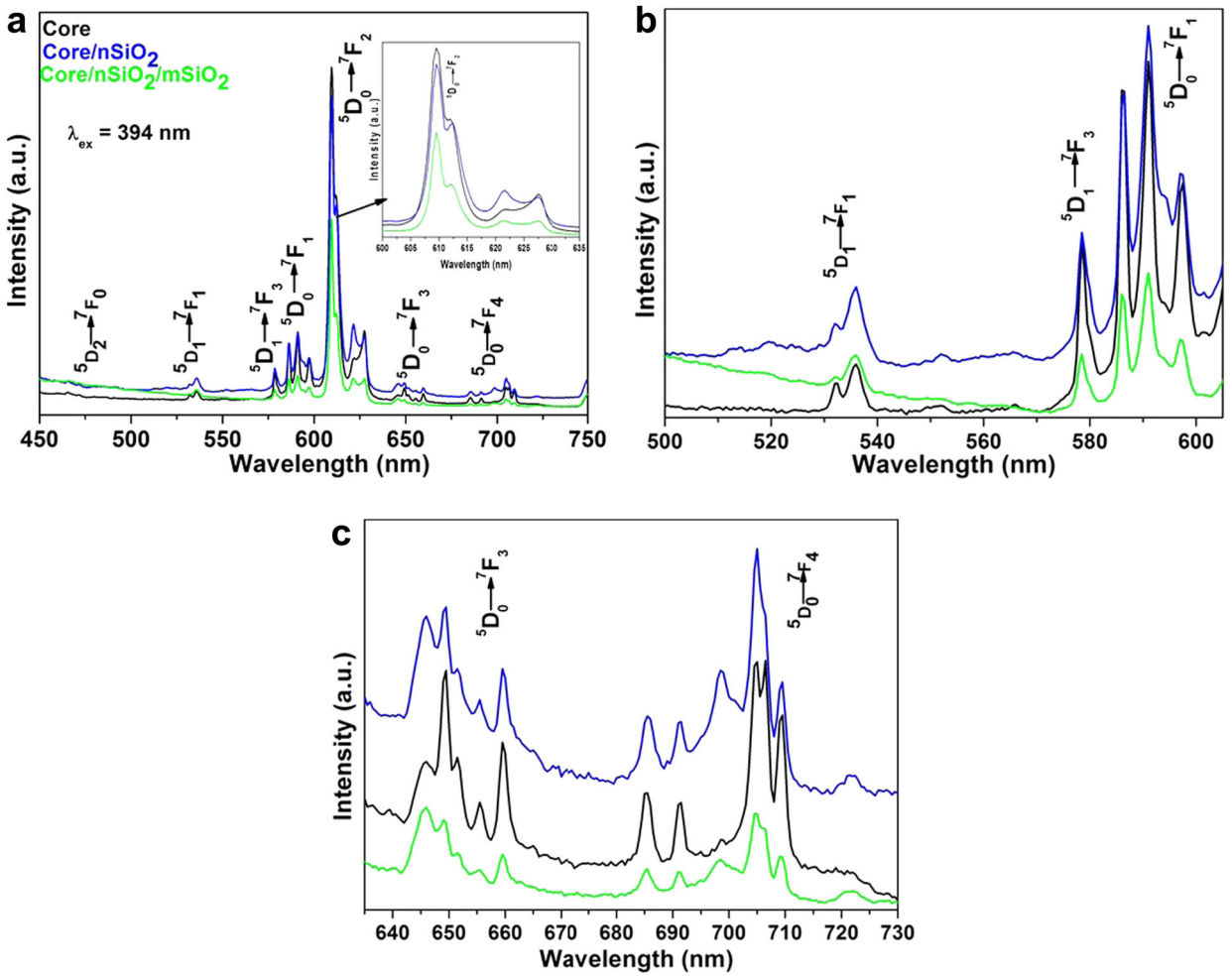

Fig. 8 Emission spectra of the as-prepared core, core/$nSiO_2$, and core/$nSiO_2$/$mSiO_2$ NPs

dipole transition is higher than their respective magnetic dipole transition; it suggests that the trivalent europium ions are in the C_2 site symmetry. We speculate that, in the cubic crystal structure of Gd_2O_3, Gd^{3+} have C_2 and S_6 symmetric site, which is both octahedral coordination. In the C_2 site, four equal equatorial Gd–O and two apical Gd–O bonds have different bond distances. However, the S_6 site has equal bond distances (Gd–O) and inversion center [6, 37, 57–59, 62]. In that case, if Eu(III) ions occupy the S_6 site symmetry of Gd^{3+} ions, the magnetic dipole transition will be obtained. In fact, the emission spectra simplify that most of the Eu^{3+} ions had C_2 symmetry compared to the S_6 symmetry, resulting in the predominant high emission intensity transition is achieved. It is interesting to note that the ^7F_J energy levels of Eu^{3+} split into some components under crystal field effects caused by the surrounding ions. Under C_2 site symmetry, $^5D_0 \rightarrow {}^7F_1$ and $^5D_0 \rightarrow {}^7F_2$ are split in multiple times. It could be due to the completely lifted "$2J + 1$" degeneracy of the ground state electronic configuration of Eu^{3+}. These results are in excellent agreement with the previous reports [3, 6, 30, 37, 57–59, 62]. It is worth noticing that, the emission intensity is suppressed in core/$nSiO_2$ NPs, which is further greatly quenched after mesoporous silica surface coating on the core/$nSiO_2$ NPs. The reduction in emission and excitation intensity is related to the formation of interfacial high phonon energy surface quenching sites by the amorphous silica and organic moieties as supported by EDX, TGA, and FTIR analysis. These surface formed high vibrational energy quenching sites enhanced the non-radiative transition pathways and suppressed the photoluminescence efficiency of the NPs. These results are in excellent agreement with the previously published reports [30, 50, 52, 63–66]. Additionally, the luminescent intensity is also associated with the structural characteristics such as crystal field effect that is closely related to the structure and its symmetry, oxygen vacancies, which also act as a quenching center for photoluminescence [67]. It is the fact that amorphous silica surface suppressed the

luminescence efficiency; whereas, enhanced the solubility, colloidal stability, biocompatibility, and non-toxic nature of the luminescent materials regardless non-silica modified luminescent core-NPs [30, 50, 68–70].

4 Conclusion

In conclusion, colloidal and mesoporous silica surface modified Gd_2O_3:Eu@nSiO_2@mSiO_2 NPs were successfully synthesized by urea-based thermal decomposition process, and subsequently, amorphous silica layer was developed by sol–gel chemical route. TEM images clearly revealed the successful mesoporous silica surface coating on the core NPs. Absorption spectra demonstrate the high solubility and colloidal stability, which verified from zeta potential results. FTIR spectral results verified the successful silica layer coating on the core NPs. The core NPs revealed strong emission transition in the red region (612 nm) even after covering of amorphous silica layer. However, the emission intensity of the silica layer cover NPs has quenched relatively their uncoated counterpart because of multiphoton-relaxation pathways from high phonon energy hydroxyl groups. These high vibrational energy groups scattered the incident and emission light, resulting to suppress the emission intensity of the nanomaterials. The available Si-OH groups on the surface enhanced the solubility, colloidal stability, biocompatibility, and non-toxic nature of the luminescent nanomaterials. Our finding illustrates the successful approach for the synthesis of very bright red phosphors for their use in broad photonic based biomedical applications like optical bio-sensor/detection/labeling, bio-imaging etc.

Acknowledgements The authors extend their appreciation to the Deanship of Scientific Research at King Saud University for funding this work through Research Group No. RG-1436-005.

Authors contributions The idea is from Dr. Ali Aldalbahi and Dr. Anees A Ansari, the manuscript was mainly written by AAA and AA. MR helped in the technical support for the characterization. All authors read and approved the final manuscript. and there is no conflict of interest.

Compliance with ethical standards

Conflict of interest The authors declare that they have no conflict of interest.

References

1. Li IF, Su CH, Sheu HS, Chiu HC, Lo YW, Lin WT, Chen JH, Yeh CS (2008) Gd2O(CO3)(2)center dot H2O particles and the corresponding Gd2O3: synthesis and applications of magnetic resonance contrast agents and template particles for hollow spheres and hybrid composites. Adv Funct Mater 18:766–776. https://doi.org/10.1002/adfm.200700702
2. Shao YZ, Tian XM, Hu WY, Zhang YY, Liu H, He HQ, Shen YY, Xie FK, Li L (2012) The properties of Gd2O3-assembled silica nanocomposite targeted nanoprobes and their application in MRI. Biomaterials 33:6438–6446. https://doi.org/10.1016/j.biomaterials.2012.05.065
3. Liu YC, Yang PP, Wang WX, Dong HX, Lin J (2010) Fabrication and photoluminescence properties of hollow Gd2O3:Ln (Ln = Eu3+, Sm3+) spheres via a sacrificial template method. Crystengcomm 12:3717–3723. https://doi.org/10.1039/c0ce00145g
4. Tian G, Gu ZJ, Liu XX, Zhou LJ, Yin WY, Yan L, Jin S, Ren WL, Xing GM, Li SJ, Zhao YL (2011) Facile fabrication of rare-earth-doped Gd2O3 hollow spheres with upconversion luminescence, magnetic resonance, and drug delivery properties. J Phys Chem C 115:23790–23796. https://doi.org/10.1021/jp209055t
5. Yang GX, Lv RC, Gai SL, Dai YL, He F, Yang PP (2014) Multifunctional SiO2@Gd2O3:Yb/Tm hollow capsules: controllable synthesis and drug release properties. Inorg Chem 53:10917–10927. https://doi.org/10.1021/ic501121t
6. Raju GSR, Pavitra E, Yu JS (2013) Facile template free synthesis of Gd2O(CO3)(2).H2O chrysanthemum-like nanoflowers and luminescence properties of corresponding Gd2O3:RE3+Spheres. Dalton Trans 42:11400–11410. https://doi.org/10.1039/c3dt51154e
7. Shi HZ, Li L, Zhang LY, Wang TT, Wang CG, Su ZM (2015) Facile fabrication of hollow mesoporous Eu3+-doped Gd2O3 nanoparticles for dual-modal imaging and drug delivery. Dyes Pigments 123:8–15. https://doi.org/10.1016/j.dyepig.2015.07.015
8. Huang CC, Liu TY, Su CH, Lo YW, Chen JH, Yeh CS (2008) Superparamagnetic hollow and paramagnetic porous Gd2O3 particles. Chem Mater 20:3840–3848. https://doi.org/10.1021/cm703195u
9. Ansari AA, Parchur AK, Alam M, Azzeer A (2014) Effect of surface coating on optical properties of Eu3+-doped CaMoO4 nanoparticles. Spectrochim Acta A 131:30–36. https://doi.org/10.1016/j.saa.2014.04.036
10. Ansari AA, Parchur AK, Alam M, Labis J, Azzeer A (2014) Influence of surface coating on structural and photoluminescent properties of CaMoO4:Pr nanoparticles. J Fluoresc 24:1253–1262. https://doi.org/10.1007/s10895-014-1409-9
11. Zhu L, Liu XM, Liu XD, Li Q, Li JY, Zhang SY, Meng J, Cao XQ (2006) Facile sonochemical synthesis of CePO4: Tb/LaPO4 core/shell nanorods with highly improved photoluminescent properties. Nanotechnology 17:4217–4222. https://doi.org/10.1088/0957-4484/17/16/036
12. Chai RT, Lian HZ, Yang PAP, Fan Y, Hou ZY, Kang XJ, Lin J (2009) In situ preparation and luminescent properties of LaPO4:Ce3+, Tb3+ nanoparticles and transparent LaPO4:Ce3+, Tb3+/PMMA nanocomposite. J Colloid Interf Sci 336:46–50. https://doi.org/10.1016/j.jcis.2009.03.079
13. Grzyb T, Weclawiak M, Lis S (2012) Influence of nanocrystals size on the structural and luminescent properties of GdOF:Eu3+. J Alloy Compd 539:82–89. https://doi.org/10.1016/j.jallcom.2012.06.047
14. Ding MY, Lu CH, Ni YR, Xu ZZ (2014) Rapid microwave-assisted flux growth of pure beta-NaYF4:Yb3+, Ln(3+) (Ln = Er, Tm, Ho) microrods with multicolor upconversion luminescence. Chem Eng J 241:477–484. https://doi.org/10.1016/j.cej.2013.10.045
15. Mi CC, Tian ZH, Han BF, Mao CB, Xu SK (2012) Microwave-assisted one-pot synthesis of water-soluble rare-earth doped fluoride luminescent nanoparticles with tunable colors. J Alloy Compd 525:154–158. https://doi.org/10.1016/j.jallcom.2012.02.095

16. Liu XX, Ni YR, Zhu C, Fang L, Kou JH, Lu CH, Xu ZZ (2016) Controllable self-assembly of NaREF4 upconversion nanoparticles and their distinctive fluorescence properties. Nanotechnology. https://doi.org/10.1088/0957-4484/27/29/295605
17. Naccache R, Vetrone F, Mahalingam V, Cuccia LA, Capobianco JA (2009) Controlled synthesis and water dispersibility of hexagonal phase NaGdF4:Ho3+/Yb3+ nanoparticles. Chem Mater 21:717–723. https://doi.org/10.1021/cm803151y
18. Chaudhary S, Kumar S, Umar A, Singh J, Rawat M, Mehta SK (2017) Europium-doped gadolinium oxide nanoparticles: a potential photoluminescencent probe for highly selective and sensitive detection of Fe3+ and Cr3+ions. Sens Actuators B 243:579–588. https://doi.org/10.1016/j.snb.2016.12.002
19. Chen GW, Qi WC, Li YB, Yang CS, Zhao XP (2016) Hydrothermal synthesis of Y2O3:Eu3+ nanorods and its growth mechanism and luminescence properties. J Mater Sci Mater Electron 27:5628–5634. https://doi.org/10.1007/s10854-016-4470-0
20. Dhananjaya N, Nagabhushana H, Nagabhushana BM, Rudraswamy B, Shivakumara C, Chakradhar RPS (2011) Hydrothermal synthesis, characterization and Raman studies of Eu3+ activated Gd2O3 nanorods. Phys B Condens Matter 406:1639–1644. https://doi.org/10.1016/j.physb.2010.09.050
21. Marques VS, Cavalcante LS, Sczancoski JC, Alcantara AFP, Orlandi MO, Moraes E, Longo E, Varela JA, Li MS, Santos MRMC (2010) Effect of different solvent ratios (water/ethylene glycol) on the growth process of CaMoO4 crystals and their optical properties. Cryst Growth Des 10:4752–4768. https://doi.org/10.1021/cg100584b
22. Runowski M, Ekner-Grzyb A, Mrowczynska L, Balabhadra S, Grzyb T, Paczesny J, Zep A, Lis S (2014) Synthesis and organic surface modification of luminescent, lanthanide-doped core/shell nanomaterials (LnF(3)@SiO2@NH2@organic acid) for potential bioapplications: spectroscopic, structural, and in vitro cytotoxicity evaluation. Langmuir 30:9533–9543. https://doi.org/10.1021/la501107a
23. Shete PB, Patil RM, Thorat ND, Prasad A, Ningthoujam RS, Ghosh SJ, Pawar SH (2014) Magnetic chitosan nanocomposite for hyperthermia therapy application: preparation, characterization and in vitro experiments. Appl Surf Sci 288:149–157. https://doi.org/10.1016/j.apsusc.2013.09.169
24. Song YH, You HP, Huang YJ, Yang M, Zheng YH, Zhang LH, Guo N (2010) Highly uniform and monodisperse Gd2O2S:Ln(3+) (Ln = Eu, Tb) submicrospheres: solvothermal synthesis and luminescence properties. Inorg Chem 49:11499–11504. https://doi.org/10.1021/ic101608b
25. Yang J, Quan ZW, Kong DY, Liu XM, Lin J (2007) Y2O3: Eu3+ microspheres: solvothermal synthesis and luminescence properties. Cryst Growth Des 7:730–735. https://doi.org/10.1021/cg060717j
26. Zhang CM, Cheng ZY, Yang PP, Xu ZH, Peng C, Li GG, Lin J (2009) Architectures of strontium hydroxyapatite microspheres: solvothermal synthesis and luminescence properties. Langmuir 25:13591–13598. https://doi.org/10.1021/la9019684
27. Jia G, You HP, Liu K, Zheng YH, Guo N, Zhang HJ (2010) Highly uniform Gd2O3 hollow microspheres: template-directed synthesis and luminescence properties. Langmuir 26:5122–5128. https://doi.org/10.1021/la903584j
28. Jia GA, You HP, Song YH, Huang YJ, Yang M, Zhang HJ (2010) Facile synthesis and luminescence of uniform Y2O3 hollow spheres by a sacrificial template route. Inorg Chem 49:7721–7725. https://doi.org/10.1021/ic100430g
29. Ansari AA, Alam M, Labis JP, Alrokayan SA, Shafi G, Hasan TN, Syed NA, Alshatwi AA (2011) Luminescent mesoporous LaVO4:Eu3+ core–shell nanoparticles: synthesis, characterization, biocompatibility and their cytotoxicity. J Mater Chem 21:19310–19316. https://doi.org/10.1039/c1jm12871j
30. Ansari AA, Labis JP, Manthrammel MA (2017) Designing of luminescent GdPO4:Eu@LaPO4@SiO2 core/shell nanorods: synthesis, structural and luminescence properties. Solid State Sci 71:117–122. https://doi.org/10.1016/j.solidstatesciences.2017.07.012
31. Slowing II, Trewyn BG, Lin VSY (2007) Mesoporous silica nanoparticles for intracellular delivery of membrane-impermeable proteins. J Am Chem Soc 129:8845–8849. https://doi.org/10.1021/ja0719780
32. Ansari AA, Hasan TN, Syed NA, Labis JP, Parchur AK, Shafi G, Alshatwi AA (2013) In-vitro cyto-toxicity, geno-toxicity, and bio-imaging evaluation of one-pot synthesized luminescent functionalized mesoporous SiO2@Eu(OH)(3) core-shell microspheres. Nanomed Nanotechnol Biol Med 9:1328–1335. https://doi.org/10.1016/j.nano.2013.05.006
33. Ansari AA, Labis JP (2012) One-pot synthesis and photoluminescence properties of luminescent functionalized mesoporous SiO2@Tb(OH)(3) core-shell nanospheres. J Mater Chem 22:16649–16656. https://doi.org/10.1039/c2jm33583b
34. Radu DR, Lai CY, Jeftinija K, Rowe EW, Jeftinija S, Lin VSY (2004) A polyamidoamine dendrimer-capped mesoporous silica nanosphere-based gene transfection reagent. J Am Chem Soc 126:13216–13217. https://doi.org/10.1021/ja046275m
35. Luo Z, Cai KY, Hu Y, Zhao L, Liu P, Duan L, Yang WH (2011) Mesoporous silica nanoparticles end-capped with collagen: redox-responsive nanoreservoirs for targeted drug delivery. Angew Chem Int Ed 50:640–643. https://doi.org/10.1002/anie.201005061
36. Paek J, Lee CH, Choi J, Choi SY, Kim A, Lee JW, Lee K (2007) Gadolinium oxide nanoring and nanoplate: anisotropic shape control. Cryst Growth Des 7:1378–1380. https://doi.org/10.1021/cg070229r
37. Gaspar RDL, Mazali IO, Sigoli FA (2010) Particle size tailoring and luminescence of europium(III)-doped gadolinium oxide obtained by the modified homogeneous precipitation method: dielectric constant and counter anion effects. Colloids Surf A 367:155–160. https://doi.org/10.1016/j.colsurfa.2010.07.003
38. Guo HC, Idris NM, Zhang Y (2011) LRET-based biodetection of DNA release in live cells using surface-modified upconverting fluorescent nanoparticles. Langmuir 27:2854–2860. https://doi.org/10.1021/la102872v
39. Wang Y, Yang T, Ke HT, Zhu AJ, Wang YY, Wang JX, Shen JK, Liu G, Chen CY, Zhao YL, Chen HB (2015) Smart albumin-biomineralized nanocomposites for multimodal imaging and photothermal tumor ablation. Adv Mater 27: 3874. https://doi.org/10.1002/adma.201500229
40. Park JY, Baek MJ, Choi ES, Woo S, Kim JH, Kim TJ, Jung JC, Chae KS, Chang Y, Lee GH (2009) Paramagnetic ultrasmall gadolinium oxide nanoparticles as advanced T-1 MR1 contrast agent: account for large longitudinal relaxivity, optimal particle diameter, and in vivo T-1 MR images. Acs Nano 3:3663–3669. https://doi.org/10.1021/nn900761s
41. Paul N, Mohanta D (2016) Evaluation of optoelectronic response and Raman active modes in Tb3+ and Eu3+-doped gadolinium oxide (Gd2O3) nanoparticle systems. Appl Phys A. http://doi.org/1007/s00339-016-0347-6
42. Runowski M, Goderski S, Paczesny J, Ksiezopolska-Gocalska M, Ekner-Grzyb A, Grzyb T, Rybka JD, Giersig M, Lis S (2016) Preparation of biocompatible, luminescent-plasmonic core/shell nanomaterials based on lanthanide and gold nanoparticles exhibiting SERS effects. J Phys Chem C 120:23788–23798. https://doi.org/10.1021/acs.jpcc.6b06644
43. Grzyb T, Runowski M, Dąbrowska K, Giersig M, Lis S (2013) Structural, spectroscopic and cytotoxicity studies of TbF3@CeF3 and TbF3@CeF3@SiO2 nanocrystals. J Nanopart Res 15:1–15. https://doi.org/10.1007/s11051-013-1958-x
44. Runowski M, Grzyb T, Zep A, Krzyczkowska P, Gorecka E, Giersig M, Lis S (2014) Eu3+ and Tb3+ doped LaPO4 nanorods, modified with a luminescent organic compound, exhibiting

tunable multicolour emission. RSA Adv 4:46305–46312. https://doi.org/10.1039/c4ra06168c
45. Huang CC, Su CH, Li WM, Liu TY, Chen JH, Yeh CS (2009) Bifunctional Gd2O3/C Nanoshells for MR Imaging and NIR Therapeutic Applications. Adv Funct Mater 19:249–258. https://doi.org/10.1002/adfm.200801454
46. Li ZQ, Wang LM, Wang ZY, Liu XH, Xiong YJ (2011) Modification of NaYF4:Yb,Er@SiO2 Nanoparticles with Gold Nanocrystals for Tunable Green-to-Red Upconversion Emissions. J Phys Chem C 115:3291–3296. https://doi.org/10.1021/jp110603r
47. Ansari AA, Aldalbahi AK, Labis JP, Manthrammel MA (2017) Impact of surface coating on physical properties of europium-doped gadolinium fluoride microspheres. J Fluor Chem 199:7–13. https://doi.org/10.1016/j.jfluchem.2017.03.015
48. Xu ZH, Li CX, Ma PA, Hou ZY, Yang DM, Kang XJ, Lin J (2011) Facile synthesis of an up-conversion luminescent and mesoporous Gd2O3:Er3 + @nSiO(2)@mSiO(2) nanocomposite as a drug carrier. Nanoscale 3:661–667. https://doi.org/10.1039/c0nr00695e
49. Szczeszak A, Ekner-Grzyb A, Runowski M, Szutkowski K, Mrowczynska L, Kazmierczak Z, Grzyb T, Dabrowska K, Giersig M, Lis S (2016) Spectroscopic, structural and in vitro cytotoxicity evaluation of luminescent, lanthanide doped core@shell nanomaterials GdVO4:Eu(3+)5%@SiO2@NH2. J Colloid Interf Sci 481:245–255. https://doi.org/10.1016/j.jcis.2016.07.025
50. Grzyb T, Runowski M, Dabrowska K, Giersig M, Lis S (2013) Structural, spectroscopic and cytotoxicity studies of TbF3@CeF3 and TbF3@CeF3@SiO2 nanocrystals. Journal of Nanoparticle Research 15. UNSP 195810.1007/s11051-013-1958-x
51. Ansari AA, Yadav R, Rai SB (2016) Enhanced luminescence efficiency of aqueous dispersible NaYF4:Yb/Er nanoparticles and the effect of surface coating. RSC Adv 6:22074–22082. https://doi.org/10.1039/c6ra00265j
52. Ansari AA, Parchur AK, Kumar B, Rai SB (2016) Influence of shell formation on morphological structure, optical and emission intensity on aqueous dispersible NaYF4:Ce/Tb nanoparticles. J Fluoresc 26:1151–1159. https://doi.org/10.1007/s10895-016-1824-1
53. Ansari AA, Manthrammel MA (2017) Surface coating effect on structural, optical and photoluminescence properties of Eu3+ doped yttrium fluoride nanoparticles. J Inorg Organomet Polym Mater 27:194–200. https://doi.org/10.1007/s10904-016-0463-y
54. Lechevallier S, Lecante P, Mauricot R, Dexpert H, Dexpert-Ghys J, Kong HK, Law GL, Wong KL (2010) Gadolinium-Europium carbonate particles: controlled precipitation for luminescent biolabeling. Chem Mater 22:6153–6161. https://doi.org/10.1021/cm102134k
55. Ren H, Zhang LY, Wang TT, Li L, Su ZM, Wang CG (2013) Universal and facile synthesis of multicolored upconversion hollow nanospheres using novel poly(acrylic acid sodium salt) microspheres as templates. Chem Commun 49:6036–6038. https://doi.org/10.1039/c3cc41284a
56. Kang JG, Min BK, Sohn Y (2015) Synthesis and characterization of Gd(OH)(3) and Gd2O3 nanorods. Ceram Int 41:1243–1248. https://doi.org/10.1016/j.ceramint.2014.09.053
57. Li JG, Zhu Q, Li XD, Sun XD, Sakka Y (2011) Colloidal processing of Gd2O3:Eu3+ red phosphor monospheres of tunable sizes: solvent effects on precipitation kinetics and photoluminescence properties of the oxides. Acta Mater 59:3688–3696. https://doi.org/10.1016/j.actamat.2011.03.004
58. Macedo AG, Ferreira RAS, Ananias D, Reis MS, Amaral VS, Carlos LD, Rocha J (2010) Effects of phonon confinement on anomalous thermalization, energy transfer, and upconversion in Ln(3+)-doped Gd2O3 nanotubes. Adv Funct Mater 20:624–634. https://doi.org/10.1002/adfm.200901772
59. Xu ZH, Gao Y, Huang SS, Ma PA, Lin J, Fang JY (2011) A luminescent and mesoporous core-shell structured Gd2O3:Eu3+@nSiO(2)@mSiO(2) nanocomposite as a drug carrier. Dalton Trans 40:4846–4854. https://doi.org/10.1039/c1dt10162e
60. Ansari AA, Labis JP (2012) Preparation and photoluminescence properties of hydrothermally synthesized YVO4:Eu3+ nanofibers. Mater Lett 88:152–155. https://doi.org/10.1016/j.matlet.2012.08.033
61. Ansari AA, Labis JP, Alrokayan SAH (2012) Synthesis of water-soluble luminescent LaVO4:Ln(3+) porous nanoparticles. J Nanopart Res. https://doi.org/10.1007/S11051-012-0999-X
62. Goglio G, Kaur G, Pinho SLC, Penin N, Blandino A, Geraldes CFGC, Garcia A, Delville MH (2015) Glycine-nitrate process for the elaboration of Eu3+-doped Gd2O3 bimodal nanoparticles for biomedical applications. Eur J Inorg Chem 7:1243–1253. https://doi.org/10.1002/ejic.201402721
63. Guo KM, Li MY, Fang XL, Luoshan MD, Bai LH, Zhao XZ (2014) Performance enhancement in dye-sensitized solar cells by utilization of a bifunctional layer consisting of core shell beta-NaYF4:Er3+/Yb3+@SiO2 submicron hexagonal prisms. J Power Sources 249:72–78. https://doi.org/10.1016/j.jpowsour.2013.10.067
64. He EJ, Zheng HR, Dong J, Gao W, Han QY, Li JN, Hui L, Lu Y, Tian HN (2014) Facile fabrication and upconversion luminescence enhancement of LaF3:Yb3+/Ln(3+)@SiO2 (Ln = Er, Tm) nanostructures decorated with Ag nanoparticles. Nanotechnology. https://doi.org/10.1088/0957-4484/25/4/045603
65. Kang XJ, Cheng ZY, Li CX, Yang DM, Shang MM, Ma PA, Li GG, Liu NA, Lin J (2011) Core–shell structured up-conversion luminescent and mesoporous NaYF4:Yb3+/Er3+@nSiO(2)@mSiO(2) nanospheres as carriers for drug delivery. J Phys Chem C 115:15801–15811. https://doi.org/10.1021/jp203039t
66. Kostiv U, Patsula V, Noculak A, Podhorodecki A, Vetvicka D, Pouckova P, Sedlakova Z, Horak D (2017) Phthalocyanine-conjugated upconversion NaYF4:Yb3+/Er3+@SiO2 nanospheres for NIR-triggered photodynamic therapy in a tumor mouse model. ChemMedChem 12:2066–2073. https://doi.org/10.1002/cmdc.201700508
67. Jacobsohn LG, Bennett BL, Muenchausen RE, Tornga SC, Thompson JD, Ugurlu O, Cooke DW, Sharma ALL (2008) Multifunction Gd2O3: Eu nanocrystals produced by solution combustion synthesis: structural, luminescent, and magnetic characterization. J Appl Phys. https://doi.org/10.1063/1.2931024
68. Ansari AA, Parchur AK, Kumar B, Rai SB (2016) Highly aqueous soluble CaF2:Ce/Tb nanocrystals: effect of surface functionalization on structural, optical band gap, and photoluminescence properties. J Mater Sci. https://doi.org/10.1007/S10856-016-5791-5
69. Shi F, Zhai XS, Zheng KZ, Zhao D, Qin WP (2011) Synthesis of monodisperse NaYF4:Yb, Tm@SiO2 nanoparticles with intense ultraviolet upconversion luminescence. J Nanosci Nanotechnol 11:9912–9915. https://doi.org/10.1166/jnn.2011.5248
70. Sotiriou GA, Franco D, Poulikakos D, Ferrari A (2012) Optically stable biocompatible flame-made SiO2-coated Y2O3: Tb3+ nanophosphors for cell imaging. Acs Nano 6:3888–3897. https://doi.org/10.1021/nn205035p